Hindawi Publishing Corporation
Journal of Nanomaterials
Volume 2014, Article ID 564694, 10 pages
http://dx.doi.org/10.1155/2014/564694

Research Article

Alumina Membrane with Hour-Glass Shaped Nanochannels: Tunable Ionic Current Rectification Device Modulated by Ions Gradient

Shengnan Hou, Qinqin Wang, Xia Fan, Zhaoyue Liu, and Jin Zhai

Key Laboratory of Bio-Inspired Smart Interfacial Science and Technology of Ministry of Education, School of Chemistry and Environment, Beihang University, Xueyuan Road, No. 37, Haidian District, Beijing 100191, China

Correspondence should be addressed to Xia Fan; fanxia@buaa.edu.cn and Jin Zhai; zhaijin@buaa.edu.cn

Received 7 May 2014; Accepted 27 May 2014; Published 19 June 2014

Academic Editor: Hao Bai

A new alumina membrane with hour-glass shaped nanochannels is reported using the double-side anodization method and the subsequently in situ pore opening procedure, which is applied to develop the tunable ionic current rectification devices that were modulated by ions gradient. By regulating the pH gradient, tunable ionic current rectification properties which are mainly dependent on the asymmetric surface charge density or polarity distribution on the inner walls of the nanochannels can be obtained. The enhanced ionic current rectification properties were presented due to the synergistic effect of the voltage driven ion flow and diffusion driven ion flow with the application of pH and electrolyte concentration gradients. Therefore, such specific alumina nanochannels would be considered as a promising candidate for building bioinspired artificial ion channel systems.

1. Introduction

In living systems, with proton migration from inward to outward of biological membranes, the transmembrane proton gradient is generated and applies essential driving force for oxidative phosphorylation to promote the formation of adenosine triphosphate (ATP), which guarantees the energy requirement of life activities [1, 2]. This phenomenon demonstrates that ions gradient plays an important role in the transmembrane ion transport behaviors [3, 4]. It inspires that, for artificial nanopores and nanochannels, ions gradient can be considered as an external parameter to regulate ionic transport behaviors [5–10], build nanofluidic devices [11–13], or construct photoelectric conversion systems [14–16]. For example, Jiang's group reported a photoelectric conversion system based on smart gating proton driven nanochannels whose inspiration came from photoelectric conversion of retina [17]. García-Giménez et al. discovered that the applied pH gradient originated strong asymmetries in the distribution of fixed charges along the bacterial porin OmpF, a biological nanopore, resulting in rectified ion transport behavior [18]. This behavior shows the preferential direction for ion flow in synthetic nanochannels, which is observed as a nonlinear current-voltage signal [19]. Nanofluidic diode system was fabricated using single conically shaped nanopore by manipulating pH gradient and an enhanced current rectification was obtained comparing with the condition that there exists homogeneous electrolyte [20]. The concentration gradient dependent ionic current rectifications were reported in charged nanopores [21, 22] and homogeneous silica nanochannels [23, 24] as well. Recently, systematic studies on rectified ion transport in artificial nanochannels with both pH gradient and concentration gradient driven ion flow are of significant interests [25].

Alumina nanochannels possess many particular advantages such as repeatability, chemical stability, high pore densities, and flexibility in controlling the geometry, which makes this inorganic nanochannel as a desired candidate for artificial ion channels [26–28]. Recently, extensive efforts have been expended on controlling the asymmetric geometric structures [29, 30] and surface properties [31] to obtain the novel nanofluidic devices based on artificial alumina nanochannels. Our group has experimentally demonstrated the diode performance of the branched alumina nanochannels, which are mainly dependent on the natural asymmetric

effect of the branched structures and the surface-charge distribution on inner walls [32]. By breaking the symmetry of the cylindrical alumina nanochannels and introducing amine functional groups, a modulated rectification behavior that is responsive to pH stimuli has been constructed [33]. However, these alumina nanochannels were nearly prepared by one-side anodization process and Al substrate as well as barrier oxide layers should be removed after anodization. To develop advanced functional nanochannels, making innovation on internal configurations of alumina nanochannels is still a huge challenge.

The anodization technique allows control over the shape of the nanochannels, and in this work a double-side anodization process was applied together with an in situ pore opening procedure. A new alumina membrane with hour-glass shaped nanochannels is fabricated. Similar to previously reported single double-conical shaped nanochannel based on organic materials [34, 35], these unique nanochannels are composed of two segments of asymmetric nanochannels, whose surface properties can be simultaneously or separately modulated by external stimuli, such as pH and concentration. Herein, we utilize the specific symmetric hour-glass shaped alumina nanochannels with asymmetric ion gradients to adjust diverse surface charge properties in order to develop the asymmetric nanochannel systems that provide variety control over both the pH- and concentration-tunable ionic rectification properties.

2. Experimental

2.1. Alumina Nanochannel Fabrication Process. The hour-glass shaped alumina nanochannels were prepared by a double-side anodization method with an in situ pore opening process. Al foil (99.999% pure, 0.1 mm thick) was firstly cleaned by acetone, ethanol, and MilliQ water (18.2 MΩ) in sequence and then was electropolished in a mixture solution of $HClO_4$ and ethanol (1 : 4 in volume ratio) at 4°C under the voltage of 17 V. The first anodization step was carried out in a 0.3 M oxalic acid solution at 5°C. Each side of the Al foil was separately anodized for 1 h and then the resulting porous oxide layer was etched from Al substrate in a solution containing 6 wt% phosphoric acid and 3.5 wt% chromic acid at 90°C for 4 h. In the second step, the corresponding Al substrate with highly ordered hemispherical concaves was anodized under the same electrolyte conditions as the first anodization. The duration of the second anodization was varied from 7 to 9.2 h in order to investigate the effect of anodization time on the growth behavior of the Al_2O_3 nanotube arrays. Here, two layers of Al_2O_3 nanotube arrays synchronously grew on both sides of the Al substrate that contact the electrolyte during anodization process. When the anodized current decreased nearly to zero at 9.2 h, Al substrate was totally anodized, and two highly ordered Al_2O_3 nanotube layers were fabricated with a barrier oxide layer at each bottom of the nanotubes. These insulating layers would block direct electrical and chemical contact between the two nanotube layers. After anodization, as-fabricated Al_2O_3 nanotubes membrane was still immersed in electrolyte oxalic acid in order to penetrate the two barrier oxide layers. This in situ pore opening time should be controlled within 30 min for forming the hour-glass shaped alumina nanochannels, which would be used as an optional candidate for artificial ion channels. The detailed microstructure of the as-prepared alumina nanotubes and nanochannels was characterized with scanning electron microscopy (SEM, Hitachi, S4300).

2.2. Current-Voltage (I-V) Measurement. The ionic transport behaviors of hour-glass shaped alumina nanochannels under the pH or ionic concentration gradient conditions were investigated in an electrochemical cell. As shown in Figure S1 (supporting information in Supplementary Material available online at http://dx.doi.org/10.1155/2014/564694), alumina nanochannels membrane was mounted between two half-cells. Potassium chloride (KCl) aqueous solutions with different pH or ion concentrations were chosen as the electrolyte. The pH of the electrolyte varied from 3.0 to 11.0, which was adjusted with 0.1 M hydrochloric acid or 0.1 M potassium hydroxide solution. The concentrations of KCl electrolyte varied from 0.1 mM to 100 mM. Ag/AgCl electrodes were settled in each half-cell to apply the desired transmembrane potential. The anode faced the left side of the nanochannels and the cathode faced the right side in all measurements. *I-V* curves were measured using a Keithley 6487 picoammeter/voltage source. The voltage was stepped between −2 V and +2 V with 200 mV steps, lasting for 5 s.

3. Results and Discussions

3.1. Alumina Nanochannel Characterization. As described in experimental process, the fabrication process of the hour-glass shaped alumina nanochannel is schematically illustrated in Figure 1, which consists of five steps. Using the double-side anodizing process (from step (a) to step (d)), the double-layer alumina nanotubes were firstly fabricated with the opposite growth direction. However, there are two insulating barrier oxide layers between the bottoms of the two nanotube layers. The in situ pore opening procedure (step (e)) was carried out immediately after the anodization process. The hour-glass shaped alumina nanochannels were finally obtained. The two opening sides have the relatively large diameters depending on the anodization voltage, while the center of the nanochannels that etched from the barrier layers have the small diameters determined by the in situ pore opening time.

3.2. Microstructure and Morphology of Alumina Nanochannels. In our work, the effect of anodization time on the growth behavior of the Al_2O_3 nanotube arrays was investigated. As shown in Figures 2(a)–2(e), two layers of Al_2O_3 nanotubes synchronously grew on both sides of the Al substrate with the growth time about 7 h, 8 h, 8.5 h, 9 h, and 9.2 h, respectively. The thickness of the membrane for all samples is controlled about 95 μm. With the increase in anodization time, the thickness of the alumina nanotube layers increased gradually from 78.2 μm to 95 μm, while the thickness of Al substrate decreased correspondingly. When

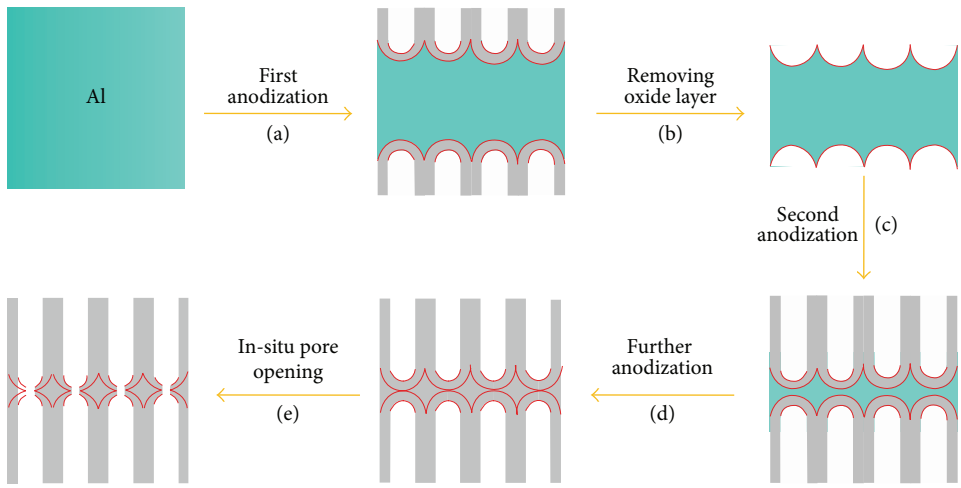

FIGURE 1: Schematic illustration of the experimental method for fabricating hour-glass shaped alumina nanochannels membrane.

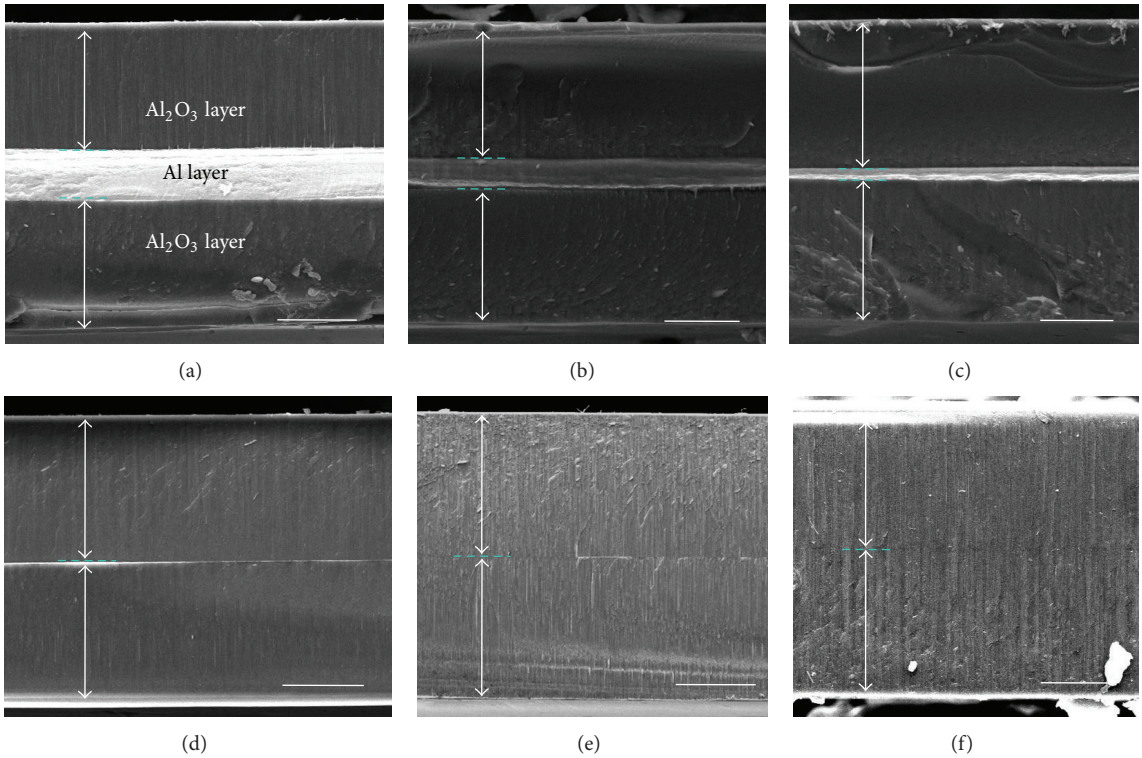

FIGURE 2: The cross-sectional SEM images of (a–e) the Al_2O_3 nanotube layers with different second-step anodized time, which would be regulated from 7 h, 8 h, 8.5 h, and 9 h to 9.2 h, respectively. The thickness of Al_2O_3 nanotube layers increased when the anodized time increased, while the thickness of Al substrate decreased. When the anodization time was 9.2 h, the Al substrate was completely anodized. The double-layer alumina nanotubes were fabricated and the boundary between the two nanotube layers became vague after 30 min in situ pore opening process (f). Scale bar is 25 μm.

the anodization time was 9 h (Figure 2(d)), Al substrate decreased to be a slice, with the thickness of about 600 nm. And finally the Al substrate was completely anodized at 9.2 h (Figure 2(e)). Then after 30 min in situ pore opening process, the boundary between two layers of alumina nanotubes became vague (Figure 2(f)). At this time, the as-fabricated alumina membrane exhibited a good transparency (Figure S2). Therefore, based on this unique phenomenon, we further investigated the detailed microstructure of the double-layer Al_2O_3 nanotubes before and after the in situ pore opening procedure.

As shown in Figures 3(a) and 3(b), pore diameters of as-prepared double-layer alumina nanotubes are about 45 nm at both top and bottom opening sides. Two barrier layers

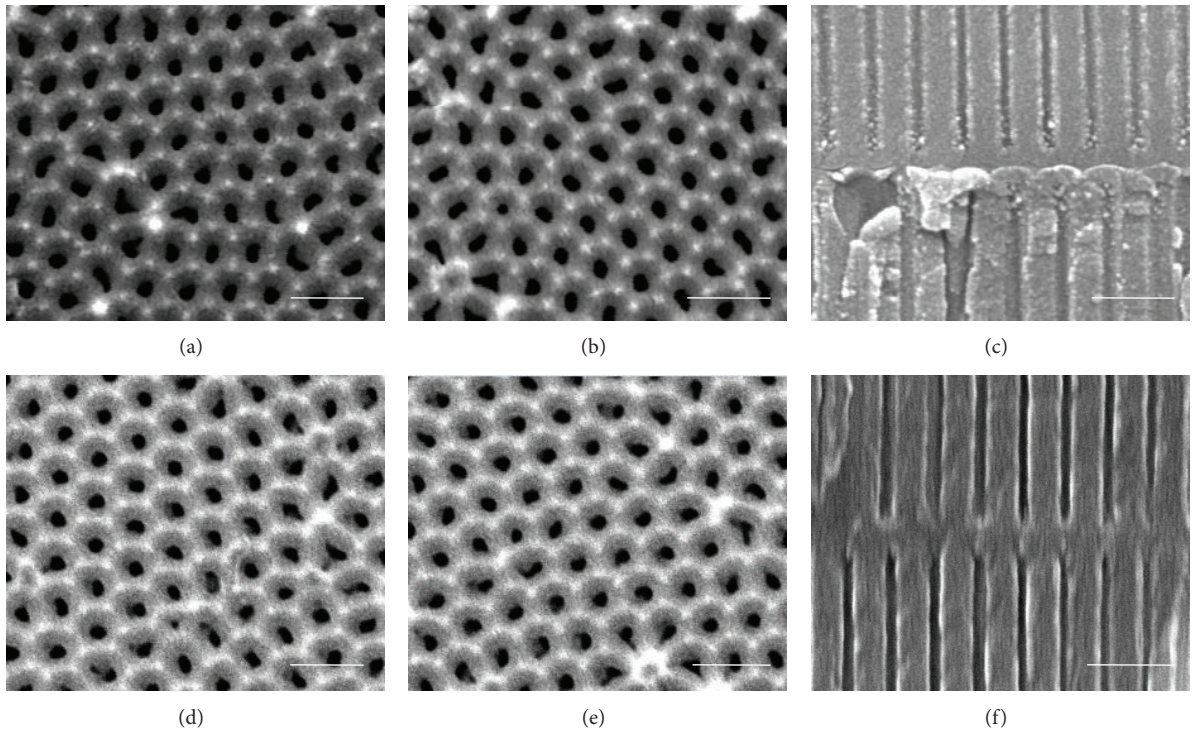

Figure 3: SEM images from the top opening side, bottom opening side, and the cross-sectional viewing of (a–c) the double-layer Al_2O_3 nanotubes and (d–f) hour-glass shaped alumina nanochannels, respectively. Both the nanotube and the nanochannel have the pore diameters at top and bottom opening sides about 45 nm. At the center of the nanotube membrane, two barrier layers closely contact and the ion transportation would be blocked. With the in situ barrier layer etching for about 30 min, hour-glass shaped nanochannel was fabricated, which has a small pore at the central region of channel with the diameter of about 15 nm. Scale bar is 200 nm.

closely contact at the center of the nanotubes membrane (Figure 3(c)). In our controlled in situ pore opening process, the inner walls of the channels would not be etched (Figures 3(d) and 3(e)), while the barrier layers were preferentially penetrated. It is clear from Figure 3(f) that an ionic confined-transportation region is observed within the nanochannels with the pore diameter about 15 nm. This in situ pore opening process is different from the wet-chemical etching methods that were usually used [36–38]. In anodization process, nanotubes growth occurred at the barrier oxide layers with the dissolving and anodizing process of Al substrate [39]. The barrier layers have the relatively higher reaction activity than the inner walls. When the anodization reaction just stopped, the alumina nanotubes membrane is nearly impassable and only a very low ion transport current was detected by *I-V* measurement (Figure S3). And then, the barrier layers would be preferably dissolved in the residual electrolyte solution because the pH value is about 0.99. Thus, the partly dissolved barrier layers resulted in the forming of hour-glass shaped nanochannels. It is noted that the inner walls can also be etched with the increase in etching time, which results in the disappearance of the confined spaces. Here, on the basis of our experimental results, the optimal in situ barrier layer etching time was determined to be 30 min for fabricating the hour-glass shaped alumina nanochannels (Figure 3(f)), which provided a desired transmembrane ionic current as the previously reported alumina nanochannels.

3.3. Influence of pH and Concentration Gradient on the Tunable Ionic Current Rectification Performances. As we know, alumina is an amphoteric material with the isoelectric point (pI) about 8.5 and the surface charges could be modulated by pH stimuli [40]. Here we present the pH-gradient dependent ionic current rectification in as-prepared hour-glass shaped alumina nanochannels. With the adjusting of pH values, the nanochannels surface carried positive ($Al\text{-}OH_2^+$) or negative charges ($Al\text{-}O^-$) due to the protonation or deprotonation of the terminated Al-OH surface. Thus, Figures 4(a) and 4(b) show the *I-V* curves of hour-glass shaped alumina nanochannels with 1 mM KCl solution under different pH gradient stimuli. The corresponding surface charge density or polarity distributions of the inner walls of alumina nanochannels are schematically represented in Figures 4(c) and 4(d) with the assumption that solutions at two half-cells meet at the central confined space of the hour-glass nanochannels. When the value of solution pH_L was 4.5 in the left half-cell, the values of pH_R in the right half-cell varied from 4.5 to 11.0 (Figures 4(a) and 4(c)). The pH gradients could be considered as four different conditions owing to the different surface charge properties on the inner walls of hour-glass shaped nanochannels. (i) Symmetric acid-acid: two asymmetric channel segments carry the same positive charges when pH 4.5 is below the pI. Undoubtedly, the linear *I-V* curve can be obtained in such symmetric hour-glass shaped alumina nanochannels, which means it does not rectify. (ii) Asymmetric acid-acid: with the

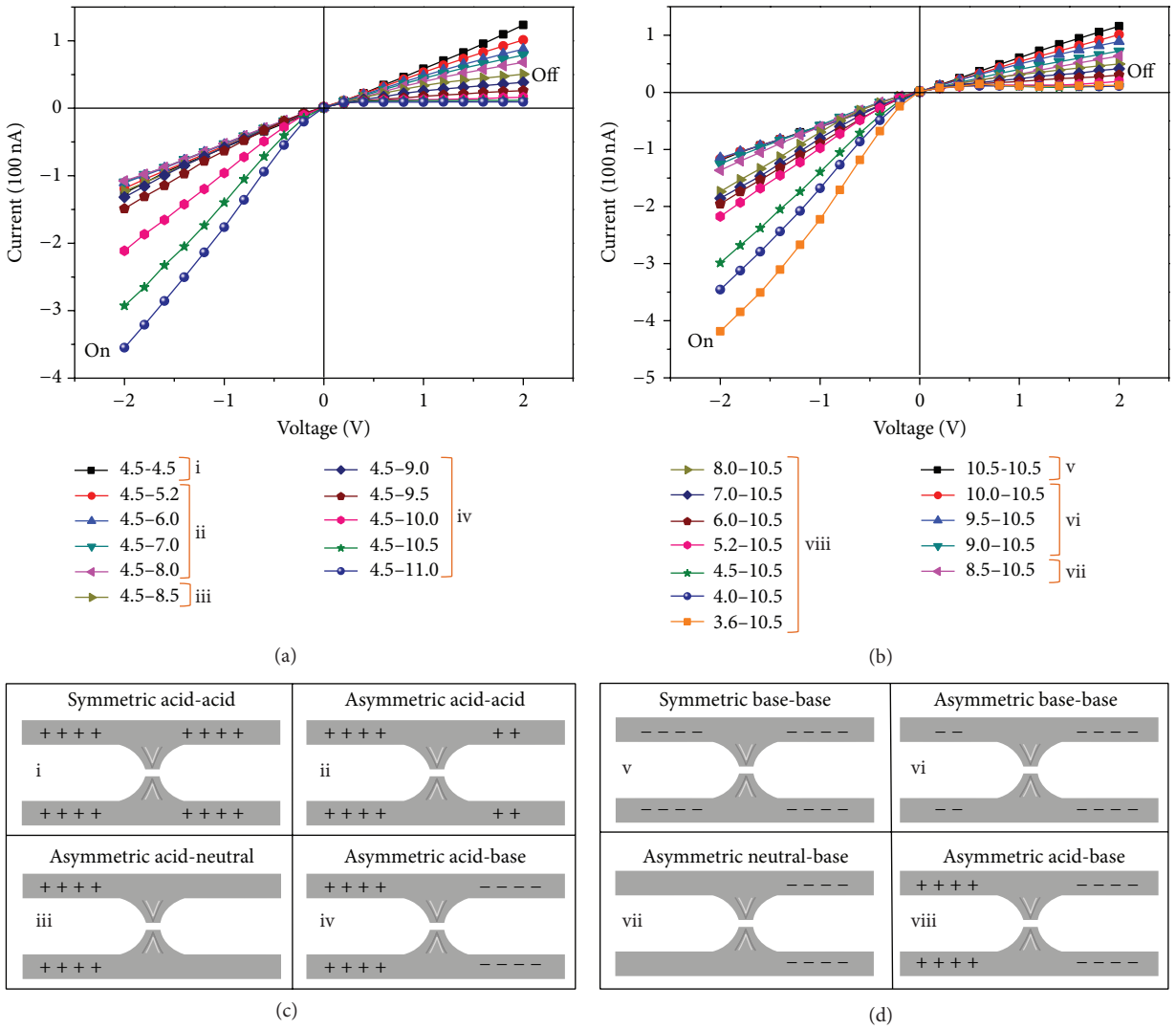

FIGURE 4: Ionic transport properties of the hour-glass shaped alumina nanochannels measured in 1 mM KCl solution with pH gradient stimuli. (a) *I-V* curves with pH_L 4.5 and pH_R varying from 4.5 to 11.0. (b) *I-V* curves with pH_R 10.5 and pH_L varying from 3.6 to 10.5. (c) and (d) schematic representation of the surface charge distribution under symmetric/asymmetric pH stimuli.

increase in pH_R values, homogeneous discontinuous positive charge density between two nanochannel segments is created. The nanochannels show the rectification characteristics as follows: a high conducting state ("on") at negative voltage and a low conducting state ("off") at positive voltage. Meanwhile, with the escalated pH gradient, the asymmetry of surface charge density distribution is enhanced, which contributes to the increase in ionic current at "on" state and the decrease in ionic current at "off" state. (iii) Asymmetric acid-neutral: only one asymmetric channel segment has the positive charges, which resulted in the nonuniform chemical composition on the symmetric nanochannels. The ionic transport condition in our experiment is relatively similar to the diode made with proteins in silicon nanochannels [41]. As a result, the rectifying occurred. (iv) Asymmetric acid-base: hour-glass shaped nanochannels have the heterogeneous surface charges, which resulted in a positive-negative charge junction like a bipolar diode [42, 43]. At negative voltage, both K^+ and Cl^- are driven toward the junction. Ions accumulated inside the electric double layer of the nanochannels dependent on the strong interaction between charged walls and ions in solution; thus, the nanochannels are the "on" state. While at positive voltage, the depletion of ions induces a low ionic current and the nanochannels are the "off" state. As a consequence, from the state (i) to state (iv), current at negative voltages dramatically increased, while it decreased at positive voltages in sequence. The best ionic rectification property was exhibited in state (iv).

Further, we investigated the rectification behaviors of hour-glass shaped alumina nanochannels with another kind of pH gradient stimuli that the pH_L values changed from 10.5 to 3.6, while the pH_R was fixed at 10.5 (Figures 4(b) and 4(d)). The pH gradients were also divided into four parts as described above including (v) symmetric base-base,

(vi) asymmetric base-base, (vii) asymmetric neutral-base, and (viii) asymmetric acid-base. The right segment nanochannels have the same negative surface charges, while the left segment nanochannels have the adjusted surface charges that vary from high negative, low negative, and neutral to positive following the pH values decreasing in sequence. It should be noted that the similar I-V curves were observed among states (i) and (v), states (ii) and (vi), states (iii) and (vii), and states (iv) and (viii), respectively. At states (vi) and (vii), the nanochannels especially exhibited the ion rectification with the same direction as states (ii) and (iii) because the surface charge polarity and the direction of the charge distribution were simultaneously reversed.

Rectification performance can be quantitatively represented by the value r, which is defined as the ratio between the currents measured at a voltage of the same amplitude but opposite polarity. In our case, the corresponding r is calculated by the absolute value of I (on state)/I (off state), measured at ±2 V applied potential. The tunable ionic rectification behavior has been represented in hour-glass shaped alumina nanochannels. Figure 5(a) shows the rectification performance of states (i), (ii), (iii), and (iv). In this case, r is 1.0 at state (i) for the symmetric pH solutions (4.5/4.5) and increases to reach the maximum value of 37.4 under the largest pH gradient (4.5/11.0) of state (iv). In Figure 5(b), when pH_R is fixed at 10.5, r is equal to 34.3 at state (viii) with asymmetric pH 3.6/10.5 stimuli and decreases to 1.0 at state (v) under the symmetric pH 10.5/10.5. So, with the increase in pH gradient, the ionic rectification behavior can be enhanced. Significant increase in rectification ratios especially is observed at states (iv) and (viii), which mainly depends on the opposite charge polarity on the asymmetric nanochannel segments. To inspect and verify the pH response of the two asymmetric alumina nanochannel segments, I-V properties of the hour-glass shaped nanochannels have been examined with asymmetric pH values changed simultaneously (Figure S4(a)). The rectification behavior can be modulated and the better rectification performance was obtained under the highest pH gradient of 3.0/11.0. The rectification ratio reaches the maximum value of 48.9 (Figure S4(b)).

Ionic concentration gradient has been identified as an important factor to influence rectification properties. We investigated the current rectification properties of hour-glass shaped alumina nanochannels under the modulating of both pH and ionic concentration gradient. Figure 6 shows the asymmetric I-V curves measured in KCl electrolyte with or without a different concentration gradient in an asymmetric acid-base solution with pH_L 5.2 and pH_R 10.0. We fixed an ionic concentration of 0.1 mM at one side and manipulated the different concentration (0.1, 1, 10, and 100 mM) at the other side. Here, ionic concentration is defined as C_L in acid solution, as well as C_R in basic solution. With the same ion concentration on both sides ($C_L = C_R = 0.1$ mM), the hour-glass shaped alumina nanochannels display an evidently asymmetric rectification behavior in the pH gradient solution. With the concentration gradient stimuli, the zero-volt current is nonzero because of the selective diffusion of the anions or cations. In addition, with the increase in the ionic concentration gradient, the negative ionic current

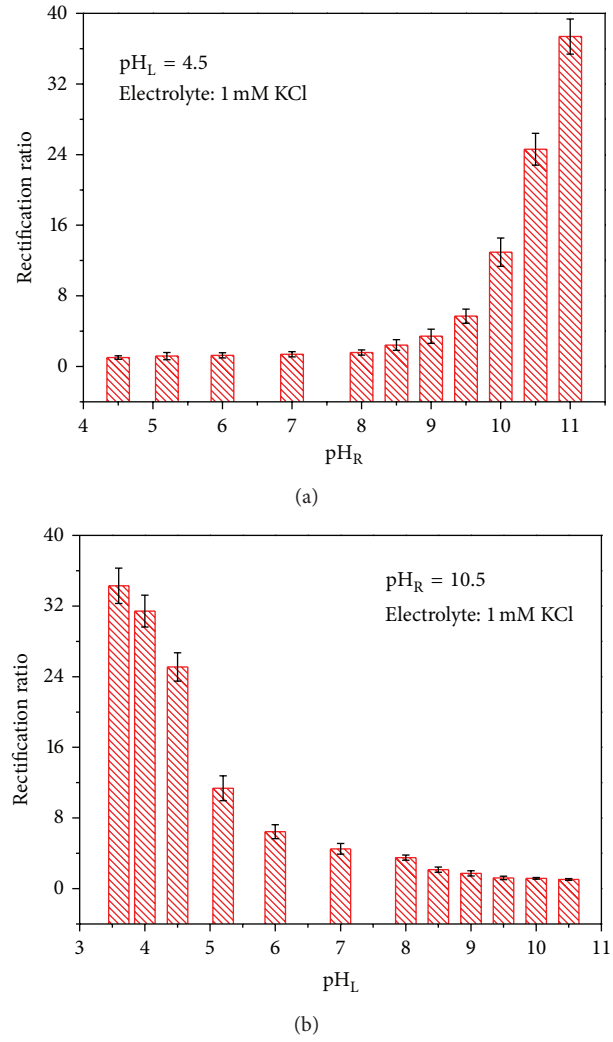

Figure 5: Ionic rectification ratio of the hour-glass shaped alumina nanochannels measured in 1 mM KCl with a series of pH gradients. (a) pH_L 4.5 and pH_R varied from 4.5 to 11.0. (b) pH_R 10.5 and pH_L varied from 3.6 to 10.5. With the increasing of pH gradient, the rectification ratios correspondingly increased.

monotonously remarkably increased ("on" state), while the positive ionic current slightly increased ("off" state).

Figure 7 illustrated how the hour-glass shaped alumina nanochannels operate under both pH and concentration gradients stimuli. Upon applying pH gradient, the ionic diode was formed, which consists of a junction between positively and negatively charged zones within the hour-glass shaped nanochannels. At the "on" state, the external voltage drives both cations (e.g., K^+) and anions (e.g., Cl^-) from the bulk solution through the nanochannel. The nanochannel has no ion selectivity and the current is carried by both cations and anions. When low ionic concentration is fixed at the acid side ($C_L < C_R$), the direction of diffusive K^+ ion flow is consistent with the voltage driven K^+ ion flow at "on" state (up-left in Figure 7), while the direction of diffusive Cl^- ion flow is opposite to the voltage driven Cl^- ion flow. As a result, the diffusion rate of K^+ along its concentration gradient

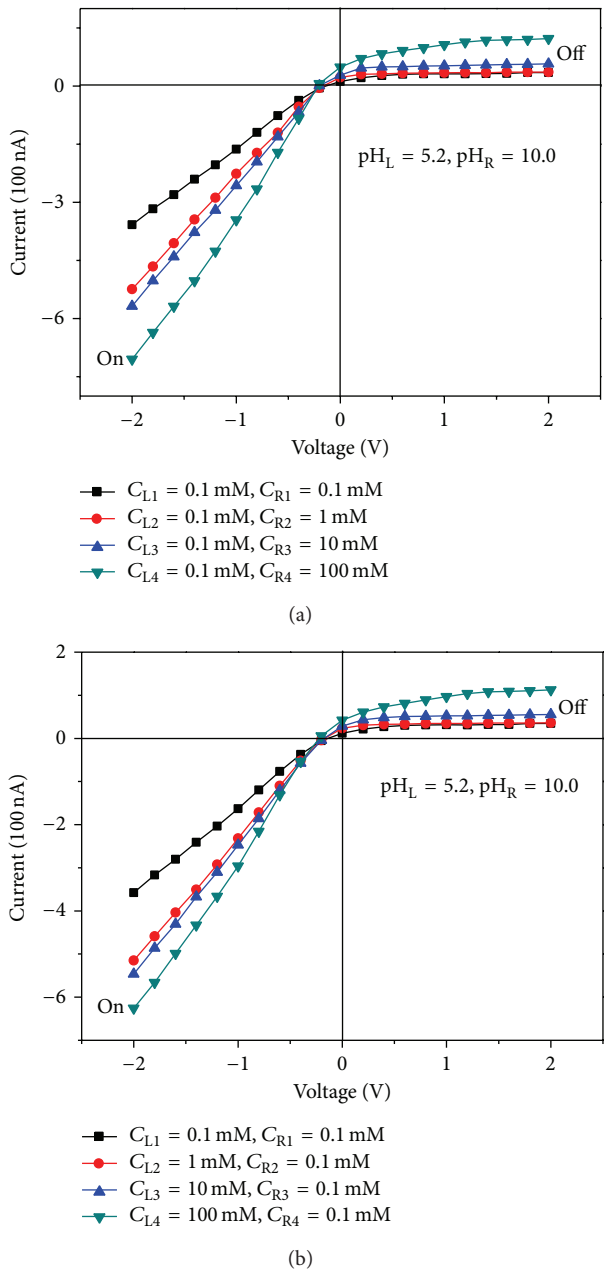

FIGURE 6: Concentration-gradient dependent ionic current rectification of hour-glass shaped alumina nanochannel in an asymmetric acid-base solution of pH$_L$ 5.2 and pH$_R$ 10.0. *I-V* curves measured in KCl electrolyte with or without a different concentration gradient. The experimental configurations are (a) C_L = 0.1 mM and C_R varied from 0.1 to 100 mM. (b) C_R = 0.1 mM and C_L changed from 0.1 to 100 mM.

(from the base side to the acid side) across the membrane is higher than the diffusion rate of Cl^-, which causes the nonzero zero-volt current. More K^+ ions are supplied from the bulk at base side than that in symmetric concentration solution and then get transported through the channel by the driven force including external bias and concentration gradient. Therefore, this forward concentration gradient contributes to a high ionic current at "on" state. At the "off" state, the voltage polarity is reversed and external bias drives ions out of the nanochannel. Under the concentration gradient stimuli, few ions can be replenished into the ion-depleted zone at base side (bottom-left in Figure 7). The diffusion of Cl^- ions from base side to the acid side would possibly occur, which results in a slightly increase in ionic current.

When low ionic concentration is fixed at base side (up-right in Figure 7), the reversed concentration gradient ($C_L > C_R$) excited a higher diffusion rate of Cl^- across the membrane from the acid side to the base side than the diffusion rate of K^+ at "on" state, which remarkably promotes the ionic currents in the same direction with the voltage driven ion flow. At the "off" state, the ion-depleted zone will be filled with the excess K^+ ions that originate from the high concentration gradient at the acid solution (bottom-right in Figure 7). Similarly, the diffusive K^+ ions may enhance the ionic transmembrane current. Therefore, regardless of the direction of the ionic concentration gradient on the forward or on the reverse, diffusive ion flow has the same ability for promoting ionic transportation properties. Ionic selective transport of the hour-glass shaped alumina nanochannels also has been constructed, which is opposite to some reported artificial nanochannels [13, 32] that asymmetric geometry is needed. Based on the regulation of both pH and concentration gradients, we implement the heterogeneous surface charges distribution and execute the asymmetric external stimuli in one integrating device successfully.

The concentration-gradient dependent ionic rectification ratios are summarized in Figure 8. Without concentration gradient, the rectification ratio of hour-glass shaped alumina nanochannels recorded at ±2 V is 10.2 under the asymmetric acid-base solution with the concentration of about 0.1 mM. When the forward concentration gradient is applied ($C_L < C_R$), the enhanced rectification ratio with a factor of 14.6 is obtained in an ionic concentration gradient of 0.1 mM/1 mM (red histogram). In this way, the diffusive ion flow remarkably promotes the ionic transport at "on" state as the synergistic effect of diffusive ion flow and voltage driven ion flow. Then, with the concentration gradient increasing to 100-fold and 1000-fold, the rectification ratios decreased to 9.9 and 5.7 due to the decrease in electrical double layer thickness in high concentrated solutions, which is not beneficial for ionic accumulated on the inner walls by the electrostatic interaction. When the reversed concentration gradient is applied ($C_L > C_R$), the optimal rectification characteristic is also obtained at 10-fold concentration gradient (grey histogram). It is affirmative that ionic rectification behavior could be enhanced under regulating of both pH and concentration gradients for such symmetric artificial nanochannels.

4. Conclusion

In summary, we fabricated a new alumina membrane with symmetric hour-glass shaped nanochannels for the first time via the double-side anodization method and an in situ pore opening procedure, which displays both pH- and concentration-modulated asymmetric ionic transport

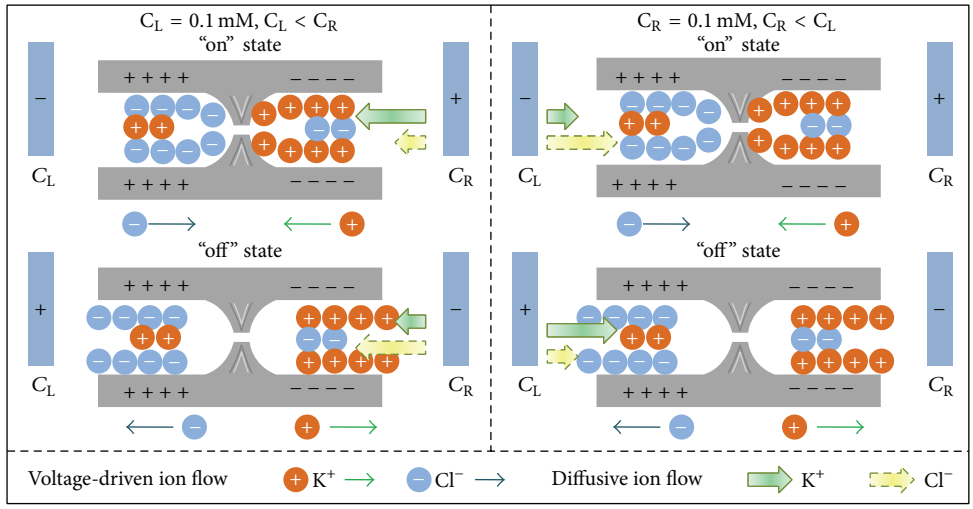

Figure 7: Schematic representation of how the alumina nanochannel operates under both pH and concentration gradient at "on" state and "off" state. When $C_L < C_R$, the direction of diffusive K^+ ion flow and voltage-induced K^+ ion flow is accordant to make large current at "on" state (up-left). While at "off" state, few Cl^- ions are replenished into the ion-depleted zone at base side and get across the membrane under the concentration gradient stimuli (bottom-left). When $C_L > C_R$, the diffusive ion flow at the acid side exhibited the same ability for promoting ionic transportation properties (right) as that at the base side. Ionic selective transport also has been constructed dependent on the cooperative effect of pH and concentration gradient. The value of pH_L is 5.2 and that of pH_R is 10.0.

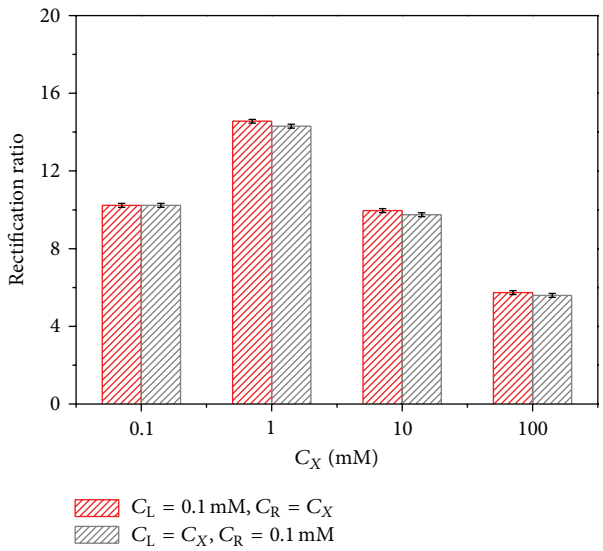

Figure 8: Ionic current rectification ratios of the hour-glass shaped alumina nanochannel with or without ionic concentration gradient. When C_L is 0.1 mM, the enhanced rectification ratio with a maximum factor of 14.6 was obtained in a 10-fold concentration gradient solution (red histogram). With this forward concentration gradient increasing to 100-fold and 1000-fold, the rectification ratios decreased. When using the reversed concentration gradient stimuli (grey histogram), we got the similar rectification ratio results. The value of pH_L is 5.2 and that of pH_R is 10.0.

properties. Under different pH gradients stimuli, the as-prepared alumina nanochannels presented regular changes in rectified ionic current on account of different surface charge density and polarity distributions on the inner walls of the nanochannels. When the pH gradient was defined, enhanced ionic current rectification properties were revealed due to the synergistic effect of the voltage driven ion flow and diffusion driven ion flow under low electrolyte concentration gradient. We believe that the hour-glass shaped alumina nanochannels may inspire innovation in the application of the complex ionic current rectification devices in contrast to previously reported nanochannels to provide molecular analysis, controlled mass transport, and photoelectric conversion systems.

Conflict of Interests

The authors declare that there is no conflict of interests regarding the publication of this paper.

Authors' Contribution

Shengnan Hou and Qinqin Wang contributed equally to this work.

Acknowledgments

The authors thank the National Natural Science Foundation of China (Grant no. 21101009) and the National Basic Research Program of China (973 Program, Grant no. 2010CB934700). The work was also supported by the Fundamental Research Funds for the Central Universities (Grant no. YWF-14-HHXY-12).

References

[1] C. Spetea and B. Schoefs, "Solute transporters in plant thylakoid membranes key players during photosynthesis and light stress,"

Communicative & Integrative Biology, vol. 3, no. 2, pp. 122–129, 2010.

[2] D. Gust, T. Moore, and A. L. Moore, "Mimicking photosynthetic solar energy transduction," *Accounts of Chemical Research*, vol. 34, no. 1, pp. 40–48, 2001.

[3] E. Gouaux and R. MacKinnon, "Principles of selective ion transport in channels and pumps," *Science*, vol. 310, no. 5753, pp. 1461–1465, 2005.

[4] H. Dong, R. Nie, X. Hou, P. Wang, J. Yue, and L. Jiang, "Assembly of F0F1-ATPase into solid state nanoporous membrane," *Chemical Communications*, vol. 47, no. 11, pp. 3102–3104, 2011.

[5] H. Zhang, X. Hou, L. Zeng et al., "Bioinspired artificial single ion pump," *Journal of the American Chemical Society*, vol. 135, no. 43, pp. 16102–16110, 2013.

[6] A. Alcaraz, P. Ramírez, E. García-Giménez, M. L. López, A. Andrio, and V. M. Aguilella, "A pH-tunable nanofluidic diode: electrochemical rectification in a reconstituted single ion channel," *The Journal of Physical Chemistry B*, vol. 110, no. 42, pp. 21205–21209, 2006.

[7] Z. S. Siwy, I. Kosińska, A. Fuliński, and C. Martin, "Asymmetric diffusion through synthetic nanopores," *Physical Review Letters*, vol. 94, no. 4, Article ID 048102, 2005.

[8] M. Ali, P. Ramirez, Q. H. Nguyen et al., "Single cigar-shaped nanopores functionalized with amphoteric amino acid chains: experimental and theoretical characterization," *ACS Nano*, vol. 6, no. 4, pp. 3631–3640, 2012.

[9] Y. He, D. Gillespie, D. Boda, I. Vlassiouk, R. S. Eisenberg, and Z. S. Siwy, "Tuning transport properties of nanofluidic devices with local charge inversion," *Journal of the American Chemical Society*, vol. 131, no. 14, pp. 5194–5202, 2009.

[10] L. H. Yeh, M. Zhang, and S. Qian, "Ion transport in a pH-regulated nanopore," *Analytical Chemistry*, vol. 85, no. 15, pp. 7527–7534, 2013.

[11] P. Ramirez, M. Ali, W. Ensinger, and S. Mafe, "Information processing with a single multifunctional nanofluidic diode," *Applied Physics Letters*, vol. 101, no. 13, Article ID 133108, 2012.

[12] J. Kim, S. J. Kim, and D. K. Kim, "Energy harvesting from salinity gradient by reverse electrodialysis with anodic alumina nanopores," *Energy*, vol. 51, pp. 413–421, 2013.

[13] I. Vlassiouk and Z. S. Siwy, "Nanofluidic diode," *Nano Letters*, vol. 7, no. 3, pp. 552–556, 2007.

[14] Z. Y. Meng, H. Bao, J. T. Wang et al., "Artificial ion channels regulating light-induced ionic currents in photoelectrical conversion systems," *Advanced Materials*, vol. 26, no. 15, pp. 2329–2334, 2014.

[15] L. P. Wen, X. Hou, Y. Tian, J. Zhai, and L. Jiang, "Bio-inspired photoelectric conversion based on smart-gating nanochannels," *Advanced Functional Materials*, vol. 20, no. 16, pp. 2636–2642, 2010.

[16] L. P. Wen, Y. Tian, Y. Guo, J. Ma, W. Liu, and L. Jiang, "Conversion of light to electricity by photoinduced reversible pH changes and biomimetic nanofluidic channels," *Advanced Functional Materials*, vol. 23, no. 22, pp. 2887–2893, 2013.

[17] W. Guo, L. C. Cao, J. Xia et al., "Energy harvesting with single-ion-selective nanopores: a concentration-gradient-driven nanofluidic power source," *Advanced Functional Materials*, vol. 20, no. 8, pp. 1339–1344, 2010.

[18] E. García-Giménez, A. Alcaraz, V. M. Aguilella, and P. Ramírez, "Directional ion selectivity in a biological nanopore with bipolar structure," *Journal of Membrane Science*, vol. 331, no. 1-2, pp. 137–142, 2009.

[19] Z. S. Siwy, "Ion-current rectification in nanopores and nanotubes with broken symmetry," *Advanced Functional Materials*, vol. 16, no. 6, pp. 735–746, 2006.

[20] L. Wang, W. Guo, Y. B. Xie, X. W. Wang, J. M. Xue, and Y. G. Wang, "Nanofluidic diode generated by pH gradient inside track-etched conical nanopore," *Radiation Measurements*, vol. 44, no. 9-10, pp. 1119–1122, 2009.

[21] L. Cao, W. Guo, Y. Wang, and L. Jiang, "Concentration-gradient-dependent ion current rectification in charged conical nanopores," *Langmuir*, vol. 28, no. 4, pp. 2194–2199, 2012.

[22] L. H. Yeh, C. Hughes, Z. Zeng, and S. Qian, "Tuning ion transport and selectivity by a salt gradient in a charged nanopore," *Analytical Chemistry*, vol. 86, no. 5, pp. 2681–2686, 2014.

[23] L. J. Cheng and L. J. Guo, "Rectified ion transport through concentration gradient in homogeneous silica nanochannels," *Nano Letters*, vol. 7, no. 10, pp. 3165–3171, 2007.

[24] W. L. Hsu, D. W. Inglis, H. Jeong et al., "Stationary chemical gradients for concentration gradient-based separation and focusing in nanofluidic channels," *Langmuir*, vol. 30, no. 18, pp. 5337–5348, 2014.

[25] I. Vlassiouk, T. R. Kozel, and Z. S. Siwy, "Biosensing with nanofluidic diodes," *Journal of the American Chemical Society*, vol. 131, no. 23, pp. 8211–8220, 2009.

[26] A. M. Md Jani, D. Losic, and N. H. Voelcker, "Nanoporous anodic aluminium oxide: advances in surface engineering and emerging applications," *Progress in Materials Science*, vol. 58, no. 5, pp. 636–704, 2013.

[27] Y. Zhou, W. Guo, J. Cheng, Y. Liu, J. Li, and L. Jiang, "High-temperature gating of solid-state nanopores with thermo-responsive macromolecular nanoactuators in ionic liquids," *Advanced Materials*, vol. 24, no. 7, pp. 962–967, 2012.

[28] Y. N. Jiang, N. Liu, W. Guo, F. Xia, and L. Jiang, "Highly-efficient gating of solid-state nanochannels by DNA super-sandwich structure containing ATP aptamers: a nanofluidic IMPLICATION logic device," *Journal of the American Chemical Society*, vol. 134, no. 37, pp. 15395–15401, 2012.

[29] R. X. Yan, W. J. Liang, R. Fan, and P. D. Yang, "Nanofluidic diodes based on nanotube heterojunctions," *Nano Letters*, vol. 9, no. 11, pp. 3820–3825, 2009.

[30] S. M. Wu, F. Wildhaber, O. Vazquez-Mena, A. Bertsch, J. Brugger, and P. Renaud, "Facile fabrication of nanofluidic diode membranes using anodic aluminium oxide," *Nanoscale*, vol. 4, no. 18, pp. 5718–5723, 2012.

[31] L. J. Cheng and L. J. Guo, "Ionic current rectification, breakdown, and switching in heterogeneous oxide nanofluidic devices," *ACS Nano*, vol. 3, no. 3, pp. 575–584, 2009.

[32] Y. Kong, X. Fan, M. H. Zhang et al., "Nanofluidic diode based on branched alumina nanochannels with tunable ionic rectification," *ACS Applied Materials & Interfaces*, vol. 5, no. 16, pp. 7931–7936, 2013.

[33] C. Y. Li, F. X. Ma, Z. Q. Wu et al., "Solution-pH-modulated rectification of ionic current in highly ordered nanochannel arrays patterned with chemical functional groups at designed positions," *Advanced Functional Materials*, vol. 23, no. 31, pp. 3836–3844, 2013.

[34] E. B. Kalman, I. Vlassiouk, and Z. S. Siwy, "Nanofluidic bipolar transistors," *Advanced Materials*, vol. 20, no. 2, pp. 293–297, 2008.

[35] X. Hou, F. Yang, L. Li, Y. Song, L. Jiang, and D. Zhu, "A biomimetic asymmetric responsive single nanochannel," *Journal of the American Chemical Society*, vol. 132, no. 33, pp. 11736–11742, 2010.

[36] H. Han, S. J. Park, J. S. Jang et al., "In situ determination of the pore opening point during wet-chemical etching of the barrier layer of porous anodic aluminum oxide: nonuniform impurity distribution in anodic oxide," *ACS Applied Materials and Interfaces*, vol. 5, no. 8, pp. 3441–3448, 2013.

[37] J. Cui, Y. Wu, Y. Wang, H. Zheng, G. Xu, and X. Zhang, "A facile and efficient approach for pore-opening detection of anodic aluminum oxide membranes," *Applied Surface Science*, vol. 258, no. 14, pp. 5305–5311, 2012.

[38] C. Y. Han, G. A. Willing, Z. L. Xiao, and H. H. Wang, "Control of the anodic aluminum oxide barrier layer opening process by wet chemical etching," *Langmuir*, vol. 23, no. 3, pp. 1564–1568, 2007.

[39] C. Cheng and A. H. W. Ngan, "Growth sustainability of nanopore channels in anodic aluminum oxide guided with prepatterns," *The Journal of Physical Chemistry C*, vol. 117, no. 23, pp. 12183–12190, 2013.

[40] M. Kosmulski, "pH-dependent surface charging and points of zero charge II. Update," *Journal of Colloid and Interface Science*, vol. 275, no. 1, pp. 214–224, 2004.

[41] R. Karnik, C. H. Duan, K. Castelino, H. Daiguji, and A. Majumdar, "Rectification of ionic current in a nanofluidic diode," *Nano Letters*, vol. 7, no. 3, pp. 547–551, 2007.

[42] H. Daiguji, Y. Oka, and K. Shirono, "Nanofluidic diode and bipolar transistor," *Nano Letters*, vol. 5, no. 11, pp. 2274–2280, 2005.

[43] Z. S. Siwy and S. Howorka, "Engineered voltage-responsive nanopores," *Chemical Society Reviews*, vol. 39, no. 3, pp. 1115–1132, 2010.